Ion Dynamics in Ionic-Liquid-Based Li-ion Electrolytes Investigated by Neutron Scattering and Dielectric Spectroscopy

Charl J. Jafta [a], Craig Bridges [a], Leon Haupt [b], Changwoo Do [c], Pit Sippel [b], Malcolm J. Cochran[c], Stephan Krohns [b], Michael Ohl [d], Alois Loidl [b], Eugene Mamontov [c*], Peter Lunkenheimer [b*], Sheng Dai [a,e*], and Xiao-Guang Sun [a*]

[a] Chemical Science Division, Oak Ridge National Laboratory, Oak Ridge, TN 37831, USA

[b] Experimental Physics V, Center for Electronic Correlations and Magnetism, University of Augsburg, 86159 Augsburg, Germany

[c] Neutron Scattering Division, Oak Ridge National Laboratory, Oak Ridge, TN 37831, USA

[d] Jülich Centre for Neutron Science, Forschungszentrum Jülich,52428 Jülich, Germany

[e] Department of Chemistry, University of Tennessee, Knoxville, TN 37996, USA

This manuscript has been authored by UT-Battelle, LLC under Contract No. DE-AC05-00OR22725 with the U.S. Department of Energy. The United States Government retains and the publisher, by accepting the article for publication, acknowledges that the United States Government retains a non-exclusive, paid-up, irrevocable, world-wide license to publish or reproduce the published form of this manuscript, or allow others to do so, for United States Government purposes. The Department of Energy will provide public access to these results of federally sponsored research in accordance with the DOE Public Access Plan (http://energy.gov/downloads/doe-public-access-plan)

Abstract

A detailed understanding of the diffusion mechanisms of ions in pure and doped ionic liquids remains an important aspect in the design of new ionic liquid electrolytes for energy storage. To gain more insight into the widely used imidazolium-based ionic liquids, we examined the relationship between viscosity, ionic conductivity, diffusion coefficients, and reorientational dynamics in the ionic liquid 3-methyl-1-methylimidazolium bis(trifluoromethanesulfonyl)imide (DMIM-TFSI) with and without lithium bis(trifluoromethanesulfonyl)imide (Li-TFSI). The diffusion coefficients for the $DMIM^+$ cation as well as the role of ion aggregates were investigated using the Quasi Elastic Neutron Scattering (QENS) and Neutron Spin Echo (NSE) techniques. Two diffusion mechanisms are observed for the $DMIM^+$ cation with and without Li-TFSI, that is, translational and local. The data additionally suggest that Li^+ ion transport along with ion aggregates, known as the vehicle mechanism, may play a significant role in the ion diffusion process. Our dielectric-spectroscopy investigations in a broad temperature and frequency range reveal a typical α-β-relaxation scenario. The α relaxation mirrors the glassy freezing of the dipolar ions while the β relaxation exhibits the signatures of a Johari-Goldstein relaxation. In contrast to the translational mode detected by neutron scattering, arising from the decoupled faster motion of the $DMIM^+$ ions, the α relaxation is well coupled to the dc charge transport, i.e., the average translational motion of all three ion species in the material. The local diffusion process detected by QENS is only weakly dependent upon temperature and viscosity and can be ascribed to the typical fast dynamics of glass-forming liquids.

Key words: Ion Dynamics, 3-methy-1-methylimidazolium bis(trifluoromethanesulfonyl)imide (DMIM-TFSI), Quasi Elastic Neutron Scattering, Neutron Spin Echo, Dielectric Spectroscopy

Introduction

Ionic liquids (ILs) are a unique class of materials having organic cations paired with inorganic or organic anions that are weakly coordinated and are defined as having a melting point below a temperature of 100 °C. These materials exhibit a characteristic set of properties, including low vapor pressure, low flammability, wide electrochemical stability windows, and high ionic conductivities, which makes them suitable as solvents for organic and inorganic synthesis, various large-scale industrial chemical processes, and as electrolytes for electric energy storage applications.[1] Although the intrinsic high ionic conductivity of ionic liquids is beneficial for energy storage applications, their cations and anions usually do not participate in the electrochemical reactions. As a result, they can potentially interfere with the electroactive species such as Li^+, Na^+, Al^{3+} etc. during the electrochemical reaction process at the electrode-electrolyte interface, as the organic cation of the ionic liquids will travel in the same direction of the electroactive cation, resulting in high polarization.[1g, 2] This is especially true when a low concentration of salt is dissolved in the IL. For example, it has been shown using the pulsed-field-gradient NMR technique, that the lithium transference number is usually below 0.1 when the molar fraction of the lithium is less than 0.2.[3] We infer that one of the effective ways to enhance lithium transference number in the IL electrolytes is to increase the molar fraction of lithium, simply by increasing the salt concentration. However, the consequence is a higher viscosity and lower ionic conductivity.[4] Given these performance tradeoffs as a function of concentration, it is crucial to understand how the ions move effectively within these ionic media. This may open a route on optimizing the structure of ILs as well as the salt concentration to improve the cycling performance of batteries using IL electrolytes.

So far, different techniques, such as molecular dynamics modeling,[4b, 5] Raman spectroscopy,[6] pulsed-field-gradient NMR,[1h, 7] electrophoretic NMR,[8] heteronuclear Overhauser NMR spectroscopy, etc.,[9] have been used to investigate the fundamental lithium transport mechanism in IL electrolytes. One common finding is a severe ion aggregation in the salt-doped IL electrolytes. In particular, Li et al. found in N-methyl-N-propylpyrrolidinium bis(trifluoromethanesulfonyl) imide (MPPy-TFSI) doped with Li-TFSI that at low salt concentration ($x \leq 0.2$) the Li^+ cation was coordinated on average by three or more $TFSI^-$ anions, with two anions contributing a single oxygen (monodendate) and one anion contributing two oxygens (bidendate).[5a] For higher salt concentration ($x \geq 0.33$) each Li^+ cation was coordinated by 3.5 anions with fewer bidendate and more monodendate anions in the Li^+ coordination sphere.[5a] In the presence of this ion aggregation, Li^+ ion transport is reported to occur *via* a combination of two mechanisms: that is, 70% through exchange of $TFSI^-$ anions between the first coordination shell and the outer coordination shells of Li^+ (structure-diffusion mechanism) and 30% through Li^+ diffusion with its coordination shell (vehicle mechanism).[5b]

In the present study, we use dielectric spectroscopy and neutron scattering techniques to help understanding the ionic dynamics in ILs with and without lithium salt doping, aiming to elucidate the role played by different diffusion mechanisms in the total ionic conductivity. Specifically, we synthesized the simplest imidazolium-based IL, 3-methyl-1-methylimidazolium bis(trifluoromethanesulfonyl) imide (DMIM-TFSI), and prepared different Li-TFSI salt concentrations in DMIM-TFSI to investigate how lithium salt affects the ion transport in the electrolyte system. We observed various dynamic processes: (i) a fast local process for $DMIM^+$, (ii) an aggregate diffusion process involving multiple ions, (iii) a dipolar relaxation process, well

coupled to the overall translational ion motion and (iv) a Johari-Goldstein relaxation as commonly found in supercooled liquids. We discuss how these processes are influenced by the salt concentration, temperature and viscosity, and show how the NSE, QENS, and dielectric spectroscopy data are both complimentary and distinct.

Experimental Section

DMIM-TFSI was synthesized and purified as reported in Ref. [10]. Li-TFSI was purchased from Aldrich and dried at 150 ^{o}C under high vacuum for 12 hours before use. Different amounts of Li-TFSI were added to DMIM-TFSI inside a glovebox to make the desired salt concentrations (molality b = 0, 0.3, 0.5, 0.7, and 1.0 mol/kg). The samples will be hereafter identified by their concentration, denoting them as 0 m, 0.3 m, etc. The viscosity was measured using a Brookfield DV-II+ Pro viscometer. The temperature was controlled using a water circulating bath, and it was given a minimum of 30 minutes for equilibration before each measurement.

Differential scanning calorimetry (DSC) was carried out with a TA Instruments DSC Q100 under nitrogen atmosphere. For each measurement the samples were tightly sealed in aluminum pans and were first equilibrated at 193 K, followed by ramping to 373 K at a heating rate of 10 K/min. The above process was then repeated from which the glass transition temperatures (T_g, onset point) and melting temperatures (T_m, peak position) were determined.

For dielectric spectroscopy, the sample material was put into parallel-plate capacitors made of stainless steel (typical diameters 5-12 mm) using glass-fiber spacers to keep the plates at a defined distance of 0.1 mm. To minimize water content, before the dielectric measurements the

prepared samples were heated at 100 °C in dry nitrogen atmosphere for up to 20 hours, which constitutes an efficient way reducing residual water.[11] During this time, the dielectric response was continuously monitored until constant values were reached, and the actual measurement run was started afterwards. For the dielectric measurements at frequencies $10^0 < \nu < 10^7$ Hz, a frequency-response analyzer (Novocontrol Alpha-analyzer) was used. Cooling and heating of the samples was achieved by a N_2-gas cryostat. Additional high-frequency measurements at $10^6 < \nu < 3\times10^9$ Hz were performed at room temperature by an I-V technique, where the sample capacitor is mounted at the end of a coaxial line, bridging inner and outer conductor.[12] For these measurements, an impedance analyzer (Agilent E4991A) was used.

The NSE experiments were carried out in the q range 0.05 $Å^{-1} \leq q \leq$ 0.3 $Å^{-1}$ with a neutron wavelength band of 6 Å ≤ λ ≤ 9 Å, for 0 m, 0.5 m, and 1.0 m ILs.[13] Aluminum sample cells were held inside a vacuum cryostat, and the temperature was controlled by a heating rod to 400 K, 425 K, and 450 K. Using polarized neutrons, the coherent scattering S(q, t)/S(q, 0) was directly measured up to Fourier times from 10 ps to 30 ns. QENS measurements were performed at the backscattering spectrometer BASIS of the Spallation Neutron Scattering facility (Oak Ridge National Laboratory) using a standard setup with an energy resolution of 3.5 µeV (full width at half maximum) and accessible range of energy transfers of ± 100 µeV.[14] IL samples with 0.0 m and 1.0 m Li-TFSI were measured on BASIS at various temperatures. Non-deuterated samples were used for both neutron scattering experiments.

Results and discussion

DSC and viscosity

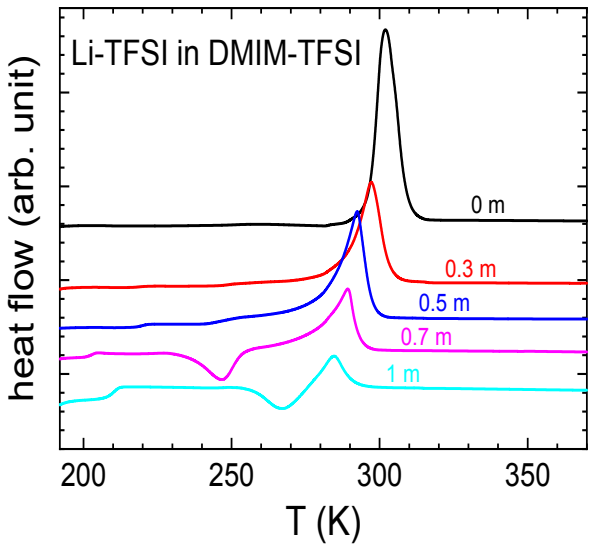

Fig. 1. Heat flow from differential scanning calorimetry for various Li-TFSI concentrations. Peaks reveal endothermic, minima exothermic transitions. Curves are shifted vertically for better readability.

The thermal properties of the DMIM-TFSI based electrolytes were evaluated using DSC (Fig. 1). For pure DMIM-TFSI, the DSC curve reveals a single endothermic peak only, with no indication of a glass-transition anomaly. Obviously, during the cooling process, DMIM-TFSI reaches a fully crystalline state whose melting leads to the endothermic peak at 302 K. A corresponding melting peak is also found for the samples with admixed Li salt. The melting point decreases to 297 K, 293 K, 289 K, and 284 K when the salt concentration increases to 0.3, 0.5, 0.7 and 1.0 m, respectively. Only for DMIM-TFSI with the highest two salt contents, significant glass-transition anomalies are detected, namely at 203 K for 0.7 m and at 208 K for 1.0 m IL. Consistent with this finding, the heat flow for these two concentrations exhibits an exothermic minimum due to crystallization, i.e., the samples indeed were (at least partly) in the glassy state after cooling.

Overall, these results reveal that, in contrast to many other ILs,[15] DMIM-TFSI cannot be easily supercooled and that its glass-forming abilities are enhanced by the admixture of the Li salt. To avoid problems with crystallization, consequently the neutron-scattering and viscosity measurements were restricted to temperatures close to and above room temperature.

Fig. 2 shows the temperature dependence of the viscosity η for the 0 m and 1 m ILs from 293 – 353 K. At 303 K, η of DMIM-TFSI without Li salt is about 32 mPas, while the 1 m IL has a higher viscosity of 63 mPas. These values are comparable to or even smaller than those for ILs typically used in lithium ion batteries.[2a, 16] The increase of viscosity with increasing Li-salt concentration can be well explained by the high ionic potential (ratio of charge to ion radius) of the Li^+ ion which should lead to increased interactions between the different ion species.

For glass-forming liquids the temperature dependence of η is often described by the Vogel-Fulcher-Tammann (VFT) equation[17]

$$\eta = \eta_0 e^{DT_0/(T - T_0)} \qquad (1)$$

where η_0 is the viscosity at infinite temperature and T_0, where $\eta(T)$ would diverge, is sometimes referred to as an "ideal" glass-transition temperature, lower than T_g.[18] The lines in Fig. 2 reveal that equation (1) provides good fits of the experimental data (see Table S1 for the parameters). The strength parameter D can be used to quantify the characteristic deviation of the system from simple thermally activated behavior, $\eta \propto \exp\,[E/(k_B T)]$, where E is an energy barrier. Generally, glass formers with high D, whose relaxation-time curves do not or only weakly deviate from linear behavior in an Arrhenius plot (log η vs. $1/T$), are termed "strong" and those that exhibit a strong curvature are termed "fragile"[17d].

Dielectric spectroscopy

As revealed by Fig. S1, in the temperature-dependence of the dielectric properties of these ILs, kinks or even jumps occur. These measurements were performed under cooling with 0.6 K/min and we ascribe this behavior to the full or partial crystallization of the samples. It becomes obvious from Fig. S1 that these anomalies are smaller for the higher salt concentrations, which is consistent with the higher tendency to supercooling for high salt contents as found in the DSC experiments (see preceding section). Especially for the 1 m sample, the kinks are nearly negligible for most frequencies and only a small part of the sample seems to crystallize, leaving most of it in the supercooled or glassy state. Thus, the detailed analysis of the frequency-dependent dielectric properties will be restricted to this sample.

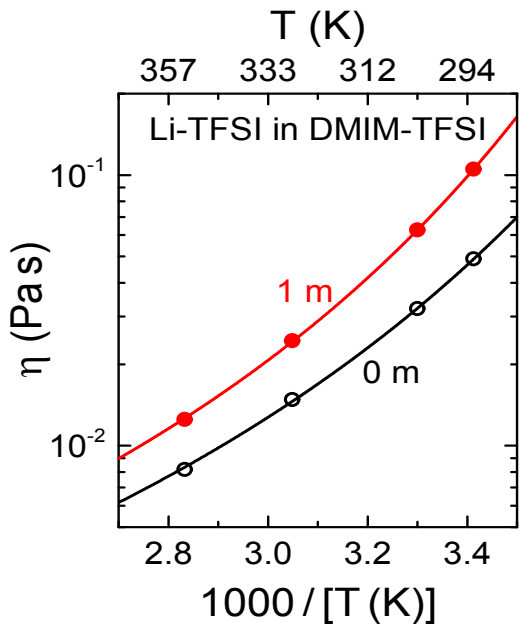

Fig. 2. Viscosity of 0 m (empty circles) and 1 m (filled circles) Li-TFSI/DMIM-TFSI as a function of the temperature (Arrhenius plot). The lines are fits with the VFT function, equation (1).

Fig. 3 shows the frequency dependence of the dielectric constant ε' (a), dielectric loss ε'' (b), and the real part of the conductivity σ' (c) of the 1 m sample. In frame (a), a strong increase of $\varepsilon'(\nu)$ with decreasing frequency is observed for temperatures $T \geq 216$ K. For low frequencies, at these temperatures the loss finally reaches values as high as 10^5 - 10^7 (see Fig. S2 representing a zoomed-out view of Fig. 3). These extremely high values obviously are of non-intrinsic origin and can be ascribed to electrode effects (also termed blocking electrodes) arising from the formation of a nearly insulating layer of immobile ions close to the sample/electrode interface.[19] This is a well-known effect for ionic conductors and will not be treated in further detail in the present work. Superimposed by this contribution, the $\varepsilon'(\nu)$ curves for 264 K $\geq T \geq$ 216 K in Fig. 3a reveal a step-like feature, which strongly shifts to lower frequencies with decreasing temperature (for lower temperatures, it is shifted out of the investigated frequency window). This is the characteristic behavior of a relaxational process involving the motion of dipolar degrees of freedom as commonly found, e.g., in dipolar supercooled liquids.[12b, 20] However, unlike the commonly observed dipolar relaxation in which the amplitude increases with cooling due to the Curie law, the amplitude of the relaxation process in Fig. 3a decreases with cooling. This is not the usual behavior of a dipolar relaxation but is often observed for the conductivity relaxation due to local ions rearrangements. Such relaxation features were also previously reported in other ILs.[21] Following previous works,[21b, 21f, 22] we ascribe the observed relaxation mode to the reorientational motions of the dipolar ions. In analogy to the main reorientational dynamics in

canonical dipolar liquids,[11] we term it α relaxation in the following. The existence of such reorientational modes in ILs has been clearly proven, e.g., by light-scattering spectroscopy.[21d, 23] It is clear that, just as for conventional dipolar liquids,[12b, 20] these modes have to lead to corresponding relaxation features in the dielectric spectra (e.g., the observed step in Fig. 3a), despite these may be difficult to discern due to the superposition by contributions from ionic conductivity (because of the general relation $\varepsilon'' \propto \sigma'/\nu$) and electrode polarization.

For relaxational processes, at the point of inflection of the relaxation step in ε', a peak should show up in the loss spectra.[12b, 20] However, in Fig. 3b this peak cannot be discerned because it is superimposed by the strong dc conductivity of this ionic conductor (the broad peaks observed at the lowest temperatures occur at clearly different frequencies than the steps in ε' and evidence a β relaxation; see next paragraph). Due to the relation $\varepsilon'' \propto \sigma'/\nu$, it leads to a dominating $1/\omega$ divergence of the loss spectra at low frequencies. In Fig. 3c, this dc conductivity is directly revealed by the clear plateau showing up in $\sigma'(\nu)$ (e.g., between about 10^2 and 10^5 Hz for the 240 K curve). The decrease of $\sigma'(\nu)$ observed at lower frequencies is due to the mentioned electrode blocking, again a well-known effect for ionic conductors.

Finally, at the lowest investigated temperatures, Fig. 3b reveals broad peaks in $\varepsilon''(\nu)$ shifting through the frequency window with temperature. They can be ascribed to a secondary relaxation process, a commonly observed phenomenon in conventional dipolar glass-forming liquids[24] and also previously observed in some ILs.[21b, 21e, 22] In Fig. 4a, a zoomed view of the loss in the region of the β relaxation is provided, including spectra at more temperatures than in Fig. 3b. As shown by Johari and Goldstein,[25] such faster processes, often termed β relaxations, seem to be a

universal feature of glass-forming matter. Various alternative microscopic explanations for the occurrence of these so-called Johari-Goldstein (JG) β relaxations have been proposed, e.g., in terms of "islands of mobility"[25] or small-angle reorientations.[26] An example for the latter are librational motions of the imidazolium ring suggested to cause β relaxations in a number of 1-hexyl-3-methylimidazolium based ILs.[21c]

As the electrode effects strongly superimpose the intrinsic response at $T \geq 216$ K, the spectra at these temperatures in Fig. 3 had to be fitted by a corresponding equivalent-circuit model to extract meaningful information on the parameters of the α relaxation. For this purpose, we modeled the blocking electrodes by up to two distributed RC circuits, connected in series to the bulk sample, as described in detail in ref. [19]. For fitting the intrinsic sample response, we assumed a Cole-Davidson (CD) function,[27] known to provide a good description of the α relaxation in many glass-forming materials[12b, 20a, 24b] and a dc-conductivity contribution, leading to $1/\nu$ behavior in ε''. The fits were performed simultaneously for ε' and ε''. As revealed by the lines in Figs. 3 and 4a and b, obviously this approach provides a reasonable description of the experimental data in the whole frequency range. The deviations seen at the highest frequencies in ε'' at 216 K are due to the onset of the β relaxation, which was not included in the fits.

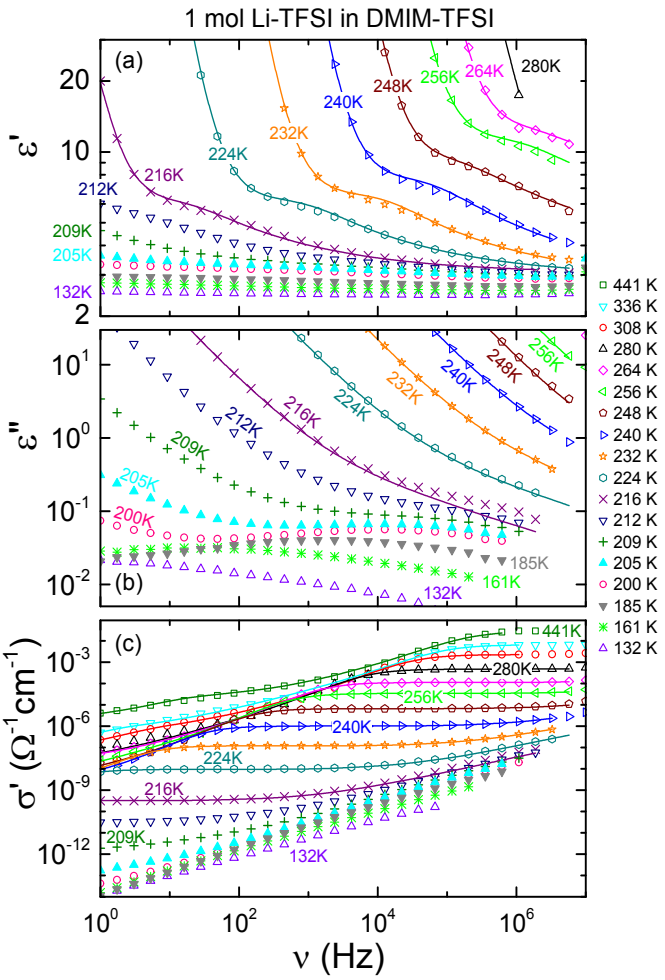

Fig. 3. Frequency dependence of the dielectric constant (a), loss (b), and conductivity (c) of DMIM-TFSI with 1 m Li-TFSI. Various spectra are shown for selected temperatures. The lines are fits of the data at $T \geq 216$ K with contributions of the dc conductivity, the α relaxation (modeled by a CD function), and up to two distributed RC circuits accounting for the blocking electrodes.[19] Frames (a) and (b) represent zoomed views of the data concentrating on the intrinsic contributions. For a view of the full spectra, see Fig. S2.

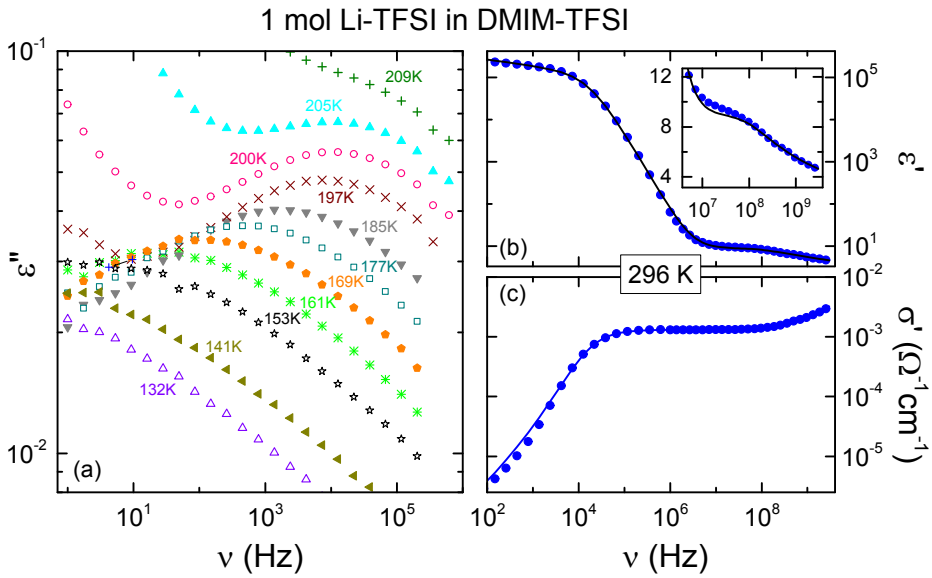

Fig. 4. (a) Frequency dependence of the dielectric loss of DMIM-TFSI with 1 m Li-TFSI. The figure provides a zoomed view of the region of the β relaxation shown for more temperatures than in Fig. 3. Frames (b) and (c) show broadband spectra of the dielectric constant and loss, respectively, taken at room temperature. The lines are fits with the same model as the fits shown in Fig. 3. The inset shows a zoomed view of the high-frequency region, where the α-relaxation step is revealed.

To reveal information on the α relaxation at room temperature, enabling a better comparison with the neutron-scattering results presented below, we performed additional high-frequency measurements extending up to 3 GHz (Fig. 4b and c). These spectra were fitted in the same way as those shown in Fig. 3 (lines in Figs. 4b and c), again leading to a reasonable description of the experimental data. As shown by the inset of Fig. 4b, the α relaxation is detected in the 100 MHz - 1 GHz range, mirroring the high dipolar mobility at room temperature. One should be aware that dielectric data of ionic conductors are sometimes analyzed in terms of the modulus formalism,[28] considering the complex dielectric modulus $M^* = 1/(\varepsilon' - i\varepsilon'')$ (see refs. [21d, 21e, 29] for some examples in ILs). In the present ILs we have at least three superimposed dynamic processes

contributing to the dielectric spectra, namely reorientational α and β relaxation and translational ion motion. Ionic charge transport is known to lead to separate peaks in M'' spectra, just as reorientational relaxation processes, which makes the proper assignment and deconvolution difficult. Moreover, the interpretation of the charge-transport related peak in M'' is rather controversial[30] and thus we refrain from providing such an analysis here. Both data representations, modulus and permittivity, of course contain the same information.

Dc conductivity

From the fits of the dielectric spectra (lines in Fig. 3) and by simply reading off the plateau values in $\sigma'(\nu)$ (Fig. 3c), the dc conductivity σ_{dc} can be determined. The results for four salt concentrations are provided in Fig. 5. The shown data are restricted to sufficiently high temperatures where (partial) crystallization of the samples, occurring especially for low salt concentrations (cf. Fig. S1), can be excluded. Generally, the ionic conductivity of any electrolyte can be described by the following equation:[31]

$$\sigma = \sum_i n_i q_i \mu_i \qquad (2)$$

where n_i, q_i and μ_i are the number, charge, and mobility of the individual charge carrier, respectively. For DMIM-TFSI, the charge carriers are the $DMIM^+$ cations and $TFSI^-$ anions, whereas for the salt-containing IL solutions the additional Li^+ cations also contribute to the charge transport. For the samples with Li-TFSI, the temperature-dependent ionic conductivity can be well described by a modified VFT equation (equation 1), replacing the viscosities η and η_0 by

conductivities σ and σ_0, respectively (solid lines in Fig. 5).[32] The 0 m IL may be better described by an Arrhenius law but the covered temperature range is too small to make a clear statement. VFT behavior of $\sigma_{dc}(T)$ is often found for ILs, mirroring the glasslike freezing of ionic dynamics.[21d, 22, 33] Fig. 5 reveals a significant decrease of the dc conductivity with increasing salt concentration. As an example, the concentration-dependent variation of σ_{dc} at room temperature is shown in the inset. It decreases roughly linearly from about 4.1×10^{-3} to 1.3×10^{-3} $\Omega^{-1}cm^{-1}$. These ionic conductivities are close to that of a conventional carbonate electrolyte used in lithium ion batteries, that is, 4.8×10^{-3} $\Omega^{-1}cm^{-1}$ for 1.0 M $LiPF_6$ dissolved in a mixture of ethylene carbonate (EC)-dimethyl carbonate (DMC)-diethyl carbonate (DEC) (1/1/1, by volume).[34] Just as the increase of viscosity (Fig. 2), the observed decrease of ionic conductivity with increasing salt concentration can be attributed to the stronger interactions between ions, caused by the introduction of the small Li^+ cation with high ionic potential, which implies a lower carrier mobility. This is consistent with the strong decrease of ionic conductivity with decreasing anion radius, reported for a number of 1-hexyl-3-methylimidazolium based ILs with identical cation and different anions.[21c] While this mechanism corresponds to a reduction of the ionic mobility μ [cf. equation (2)], an increased formation of ion aggregates triggered by the Li addition cannot be excluded[5b], which would correspond to a reduction of the number of free charge carriers n. Overall, while large ion aggregates are likely to exist in high salt concentration electrolytes, the detailed transport mechanism is still a matter of debate.

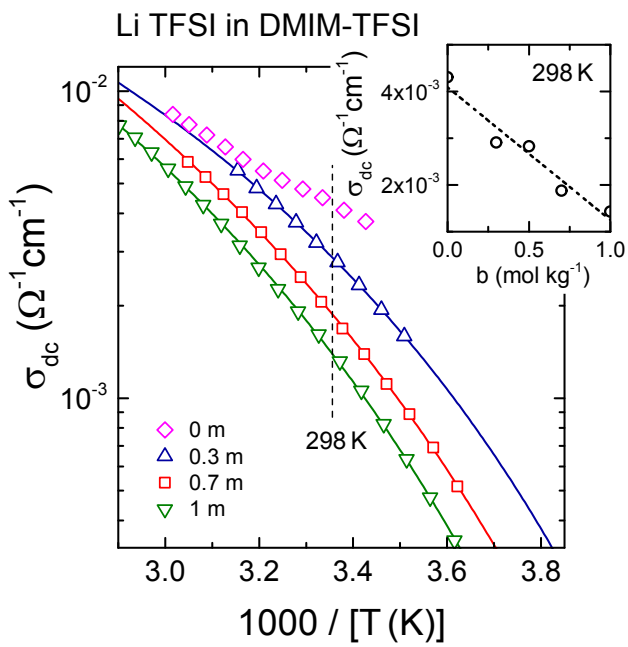

Fig. 5. The dc conductivity as a function of temperature of DMIM-TFSI without and with different salt concentration of Li-TFSI. The lines are fits with the VFT equation. The inset shows the dependence of the dc conductivity on the salt concentration; the dashed line is a linear fit.

Neutron scattering

To directly detect the ion motion and relate it to the Li^+ ion transport mechanism[35], we used QENS and NSE measurements. The signal in QENS experiments is sensitive to the incoherent neutron scattering cross section of an element. As hydrogen has an exceptionally high incoherent scattering cross section, QENS is very sensitive to hydrogen motion. For the ionic liquid DMIM-TFSI, while there are nine hydrogen atoms in the cation, there is no hydrogen present in the $TFSI^-$ anion. Thus, the diffusion coefficients calculated from the QENS data can be interpreted as self-diffusion coefficients of the $DMIM^+$ cations.

The QENS data of the 0 m and 1 m ILs at 303 K, 328 K and 353 K are shown in Fig. S3. The same data sets converted to imaginary part of the dynamic susceptibility, $I(Q,E)=S(Q,E)/(n_B(E)+1)\approx(E/k_BT)S(Q,E)$, are shown in Fig S4. The susceptibility spectra exhibit a peak at ca. 1 μeV with a fairly strong Q-dependence of the peak position, characteristic of translational diffusivity, the slowest measurable process. At ca. 10 μeV, there is a shoulder with a strong Q-dependence of intensity, characteristic of a localized mobility denoting a faster dynamic process. Finally, near the cutoff of the accessible energy transfer range of ca. 100 μeV, there is evidence of a tail of yet another dynamic process, too fast to be resolved in the current experiment, also with a fairly strong Q-dependence of intensity, characteristic of a localized mobility. The susceptibility spectra suggest that there may be two dynamic components resolvable within the dynamic range of the experiment, on the 1 μeV and 10 μeV scale, and another, much faster component, that cannot be determined reliably, but likely necessitate the use of a background term in the fits.

In a typical QENS experiment, the limited dynamic range significantly restricts the maximum number of fit parameters, oftentimes imposing a choice between a single “stretched” or two Debye-like components, as it is usually impossible to use more than one “stretched” fit component. The choice can be made either from direct comparison of fits quality, or on the grounds of the appearance of the dynamic susceptibility spectra, which sometimes could distinguish between single or double component scenarios, as is the case with the present data sets.

The formalism used for two Debye-like component analysis of QENS data from liquids has been discussed in detail in reference.[36] In brief, assuming that the faster and slower motions of hydrogen-bearing cations can be treated as independent, for each q one can write the intermediate scattering function as a simple product, $F(t) = T_1(t)T_2(t)$, and the scattering function as a convolution, $S(E)=T_1(E)\otimes T_2(E)$, where T_1 and T_2 represent different motions. One can approximate the functional form for the faster spatially constrained process by equation (3):

$$T_1(t) = p + (1-p)exp\left[-\frac{t}{\tau_1}\right] \qquad (3)$$

where τ_1 is a q-dependent relaxation time. The parameter p describes the q-dependent fraction of "elastic" scattering for the transiently constrained translational diffusion process, commonly known as Elastic Incoherent Structure Factor (EISF). If unrestricted translational diffusion involves molecules as a whole, the slower, not spatially constrained diffusion process, can be approximated by equation (4):

$$T_2(t) = exp\left[-\frac{t}{\tau_2}\right] \qquad (4)$$

where τ_2 is a q-dependent relaxation time. The convolution in the energy space is facilitated by the fact that the intermediate scattering functions that we use consist of only time-independent and exponential terms, yielding equations (5) and (6):

$$F(t) = (1-p)exp\left[-t\left(\frac{1}{\tau_1}+\frac{1}{\tau_2}\right)\right] + p\, exp\left[-\frac{t}{\tau_2}\right] \qquad (5)$$

$$S(E) = (1-p)\frac{1}{\pi}\frac{\left[\left(\hbar/\tau_1\right)+\left(\hbar/\tau_2\right)\right]}{E^2+\left[\left(\hbar/\tau_1\right)+\left(\hbar/\tau_2\right)\right]^2} + p\frac{1}{\pi}\frac{\left(\hbar/\tau_2\right)}{E^2+\left(\hbar/\tau_2\right)^2} \qquad (6)$$

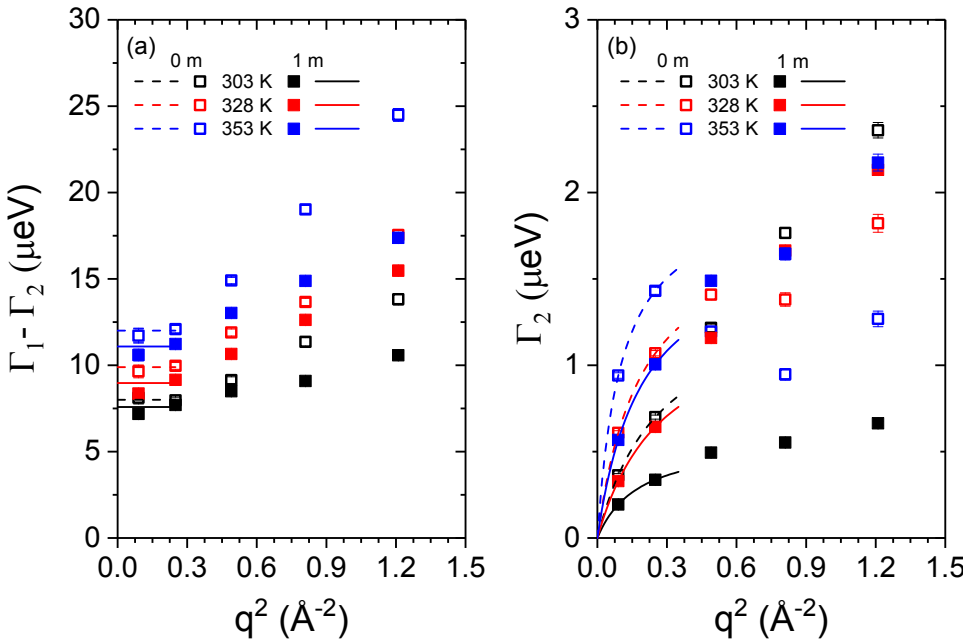

Fig. 6. Plots of the half-width half-maximum (HWHM) for (a) the broad quasi-elastic component ($\Gamma_1 - \Gamma_2$) and (b) the narrow quasi elastic component (Γ_2) as a function of q^2 for the 0 m and 1 m salt concentrations at temperatures 303 K, 328 K and 353 K. The corresponding lines are fits that are used to calculate (a) the local and (b) translational diffusion coefficient values, respectively, as described in the text.

The relaxation times for the slow process are thus directly determined from the narrow component, whereas the relaxation times pertinent to the fast process are determined from the difference in the broad and narrow component widths. As we have mentioned above, the parameter p is the EISF for the faster, transiently constrained (between the consecutive events associated with the main structural relaxation) motions of cations. Fig. 6 shows the plots of the half-widths at half-maximum (HWHM) as a function of q^2 for the 0 m and 1 m salt concentrations at different temperatures, as determined from the data fits (performed independently at each Q) with equation (7):

$$I(E) = S(E) \otimes R(E) + (CE + D) \qquad (7)$$

where the model dynamic structure factor described by Eq. (6) is convolved with the resolution function, R(E), and a linear background term is added. The HWHMs are related to the τ parameters in Eq. (6) as HWHM=(h/2π)/τ. The low q behavior of $\Gamma_1 - \Gamma_2$ shows a constant HWHM below ~0.4 Å^{-2} (see Fig. 6a), which is not observed in the low q behavior of Γ_2 (Fig. 6b), suggesting that the faster diffusion process is spatially confined, unlike the slower translational diffusion process. The translational (either locally, or for the long range) character of both processes is evident from the increasing HWHM as a function of q^2 as observed in both Fig. 6a (locally translational motion) and Fig. 6b (long-range translational motion).[36]

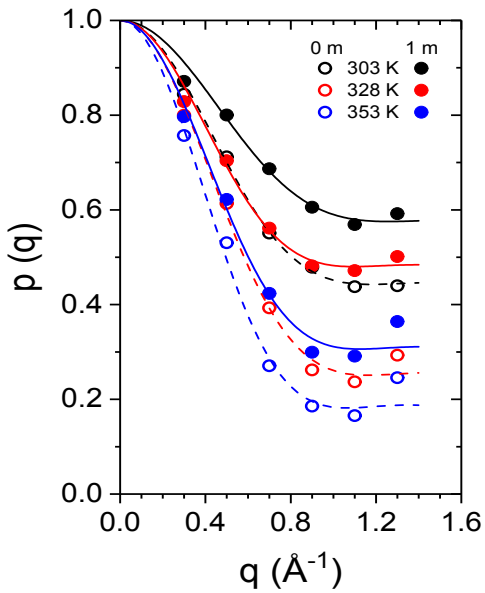

Fig. 7. Fits to the elastic incoherent structure factor (EISF) p(q) for 0 m and 1 m LiTFSI salt concentrations in DMIM.TFSI, at temperatures 303 K, 328 K and 353 K. The lines, which are fits to the experimental data points (see text), were used to determine the confinement radii for the local diffusion process identified in the QENS data.

As is appropriate for localized diffusivity[37], the faster diffusion coefficients (*D*) for $\Gamma = \Gamma_1 - \Gamma_2$ were calculated using the equation $\Gamma = {}^{4.33D}/_{a^2}$, where a is the confinement radius, and where $\Gamma_1 - \Gamma_2$ was taken as the average of the first two *q* points as shown by the horizontal lines in Fig. 6a. The confinement radius a was determined from fitting the q-dependent EISF (in this case, the parameter p in equations 5 and 6) with $c_1 + (1 - c_1)\left(\frac{3j_1(qa_1)}{qa_1}\right)^2$ (Fig. 7), where j_1 is the spherical Bessel function of the first order and where c_1 describes the "immobile" fraction.[36, 38] The confinement radii for the 0 m ILs are 3.82 Å, 3.87 Å, and 4.23 Å at 303 K, 328 K, and 353 K, respectively. For the 1 m case these are 3.57 Å, 4.10 Å, and 4.00 Å for the ILs at 303 K, 328 K, and 353 K, respectively. These values were then used to calculate the local diffusion coefficients, *D*, associated with the fast component from $\Gamma = {}^{4.33D}/_{a^2}$. Fig. 8a shows the temperature dependence of the obtained diffusion coefficients of the faster process (squares), which we assign to a local (confined) process (i.e., motion in the transient cage of the nearest neighbors). These calculated diffusion coefficients, revealing slightly lower values for the 1 m IL, are also listed in Table 1. Similar values have been observed in other IL systems.[10a]

For the slow component, the translational diffusion coefficient *D* can be determined from the low *q* data using jump diffusion model, $HWHM(Q)=(h/2\pi\tau)(DQ^2/(1+\tau DQ^2)$ (see lines in Fig. 6b). The calculated coefficients, plotted in Fig. 8a (triangles) and listed in table 1, again are slightly lower for the 1 m IL. For both IL samples (0 m and 1 m), the local diffusion coefficients are nearly an order of magnitude higher than the translational diffusion coefficients, as may be expected for a shorter ranged process. The temperature dependence of the local diffusion coefficients in both 0 m and 1 m ILs is significantly weaker than that of the translational diffusion coefficients.

The local diffusion is relatively independent of the salt concentration and, thus, of the bulk viscosity of the IL, as compared to the translational diffusion, which again may be expected considering the length scale of the process.

Comparison can be made with the translational diffusion coefficient of the $DMIM^+$ cation in DMIM-TFSI of $\sim 1 \times 10^{-10}\, m^2/s$ at 328 K, deduced from NMR measurements reported in the literature, which is consistent with that calculated from the QENS data.[10a] Triolo et al. similarly reported that there are two distinct processes in the ionic liquid BMIM-PF_6, labelled as α- and β-process; they determined that the faster β-process, ascribed to "localized vibrational motions", is essentially temperature independent (250 K – 320 K), where our faster process is weakly temperature dependent.[39] It should be noted that caged dynamics, arising from fast motions of the molecules or ions in cages formed by the nearest neighbors, is often termed β relaxation in literature, just as the JG β process discussed above.[12b, 40] However, both are not related, the latter usually arising at much lower frequencies, typically in the Hz - MHz regime.[24]

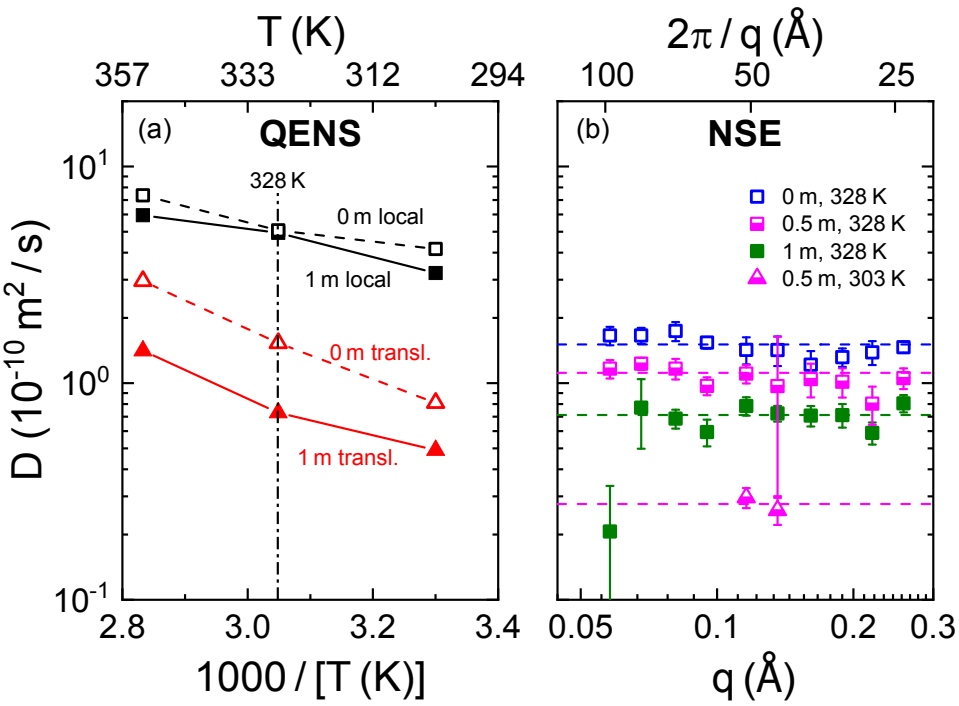

Fig. 8. (a) Temperature dependence of the diffusion coefficients of the DMIM-TFSI ILs without and with 1 m Li salt, deduced from the QENS measurements (Arrhenius representation). The solid and dashed lines connect the data points. There are two processes, ascribed to local and translational diffusion. (b) Momentum-transfer dependence of the diffusion coefficients at 328 K as determined from the NSE experiments. Results are shown for three Li-salt concentrations. For the 0.5 m sample, additional data at 303 K are provided. A single process, proposed to be of translational nature, is observed.

Table 1: The diffusion coefficients calculated from QENS and NSE.

	LiTFSI concentration	**0 m**			**0.5 m**		**1m**		
	Temperature (K)	**303**	**328**	**353**	**303**	**328**	**303**	**328**	**353**
QENS	Local diffusion coefficients ($\times 10^{-10}$ m^2/s)	4.16	5.07	7.36	-	-	3.22	4.94	5.95
	Translation diffusion coefficients ($\times 10^{-10}$	0.81	1.53	2.96	-	-	0.49	0.73	1.41

	m^2/s)								
NSE	Average (over q) diffusion coefficients ($\times 10^{-10} m^2/s$)	-	1.51	-	0.28	1.11	-	0.71	-

Generally, NSE spectroscopy should probe the dynamics of the whole DMIM-TFSI system, including cation, anion, and ion aggregates. However, when considering that the neutron scattering cross-section of $TFSI^-$ and Li^+ are much smaller as compared to $DMIM^+$, the diffusion coefficients calculated from NSE are also dominated by the $DMIM^+$ dynamics. The NSE measurements are capturing slower dynamics at a longer length scale (q < 0.3 $Å^{-1}$) than the QENS experiments, and so only one translational diffusion process is observed. As revealed by Fig. 8b, showing the dependence on momentum transfer for the 0 m, 0.5 m, and 1 m ILs, the diffusion coefficients are essentially independent of the length scale measured, but they show a significant trend with respect to temperature and salt concentration. The average diffusion coefficients (average in q) of the 0 m, 0.5 m, and 1 m ILs at 328 K are listed in table 1. We note that the 0.5 m IL average diffusion coefficients calculated from the NSE data at 303 K are significantly lower than those at 328 K, indicating that the diffusion is much more strongly influenced by temperature than by salt concentration. The NSE data confirm that the slower diffusion process measured by QENS corresponds to longer-range translational diffusion, with very similar diffusion coefficients determined independently by these different scattering techniques. When the salt concentration increases from 0 m to 1 m at 328 K, the diffusion coefficients calculated from the QENS and NSE data decrease by 46 % and 53 %, respectively. One possible explanation for the slight difference

between the NSE and QENS data in terms of the magnitude of the translational diffusion process is that the QENS data are self-diffusion coefficients of the $DMIM^+$ cations, whereas the additional 7 % decrease in the NSE data can be attributed to the ion aggregates.

Comparison of relaxation times, resistivity, and viscosity

Fig. 9 shows an Arrhenius representation of the temperature-dependent relaxation times of the IL with 1 m Li-TFSI as deduced in the present work (left scale). The squares show the dielectric α-relaxation time $\tau_{\alpha,\mathrm{diel}}$, determined from the fits shown in Figs. 3, 4b and c, and S2. It exhibits clear deviations from simple thermally activated temperature dependence, $\tau \propto \exp[E/(k_B T)]$ (with E an energy barrier) revealed by its significantly non-linear behavior in the Arrhenius plot. This is a common phenomenon of glass-forming liquids, often ascribed to an increase of molecular cooperativity with decreasing temperature,[17e, 18a, 41] and is also often found in ILs.[21b-d, 22, 29a] In Fig. 9, $\tau_{\alpha,\mathrm{diel}}$ is compared to the dc resistivity ρ_{dc}, also determined from the fits of the dielectric spectra (circles; right scale). The high-temperature part of these data (shown as $\sigma_{\mathrm{dc}} = 1/\rho_{\mathrm{dc}}$) was already presented in Fig. 5. Obviously, both data sets can be well scaled onto each other, i.e., they are proportional, $\tau_{\alpha,\mathrm{diel}} \propto \rho_{\mathrm{dc}}$ (note that the total number of decades is identical for both ordinates in Fig. 9 and only the starting value of the ordinate was adapted for the scaling). This finding implies a close coupling of the translational ionic motion and the reorientational motion of the dipolar ions in this IL. Such coupling is also found in molecular glass formers with admixed ionic charge carriers[42] and even in ionically conducting plastic crystals.[43]

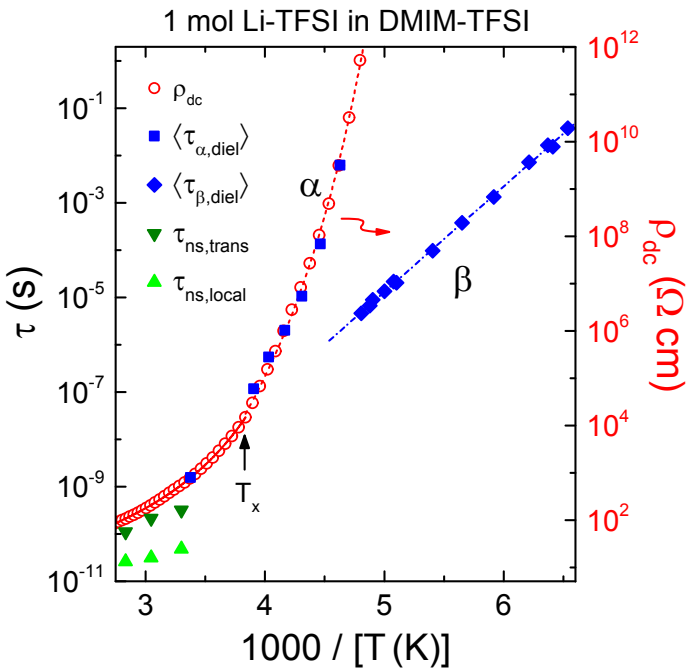

Fig. 9. Comparison of the temperature dependences of the relaxation times of DMIM-TFSI mixed with 1 m Li-TFSI (left scale) and of its dc resistivity (circles; right scale), shown in Arrhenius representation. The figure includes the average α- and β-relaxation times determined from dielectric spectroscopy (squares and diamonds, respectively) and τ, calculated by $\frac{1}{Dq^2}$ with q = 0.8 Å^{-1}, of the two processes detected by neutron scattering (triangles). The vertical arrow indicates the temperature T_x = 261 K below which partial crystallization may have occurred (cf. Fig. S1). The solid and dashed lines are fits of $\rho(T)$ above and below T_x, respectively, using the VFT equation. The dash-dotted line is a linear fit, corresponding to Arrhenius behavior.

The ρ_{dc}(T) data cover the broadest and most continuous temperature range of all dynamic quantities deduced in the present work (cf. Figs. 9 and 10). Its range is also larger than that of $\tau_{\alpha,\mathrm{diel}}(T)$ because the dc plateau in $\sigma'(\nu)$ can be read off even when the α relaxation has shifted out of the frequency window (Fig. 9). However, as discussed above and signified by the temperature-dependent dielectric properties shown in Fig. S1, even the 1 m sample seems to exhibit partial crystallization at $T_x \approx$ 261 K, whatsoever much less pronounced than for the other

concentrations. Nevertheless, the temperature dependence of ρ_{dc} in Fig. 9 at first glance appears smooth and not affected by crystallization. However, a closer look reveals a small change of slope at T_x, indicated by the vertical arrow. Therefore, these data were fitted by two separate VFT laws [equation (1) with η replaced by ρ_{dc}] above and below T_x. The fits are shown by the solid and dashed lines in Fig. 9, leading to a nearly perfect description of the experimental data.

Fig. 10 shows an Arrhenius plot of the high-temperature region of ρ_{dc}(T) for the 1m IL (closed circles; right scale), together with the viscosity data already provided in Fig. 2 (closed stars; leftmost scale). Obviously, both quantities also can be scaled onto each other and, thus, we have $\eta \propto \rho_{dc} \propto \tau_{\alpha,\mathrm{diel}}$ for this material. The close coupling of these different dynamic quantities indicates that the temperature dependence of the resistivity (or of the conductivity) is dominated by dynamics, i.e., by the temperature dependence of the mobility μ in equation (2). In contrast, based on these findings, a temperature-dependent variation of the number of free charge-carriers n, which could arise from a temperature-dependent variation of the number of cation-anion pairs or aggregates (causing a temperature dependence of the so-called ionicity)[44], seems unlikely.

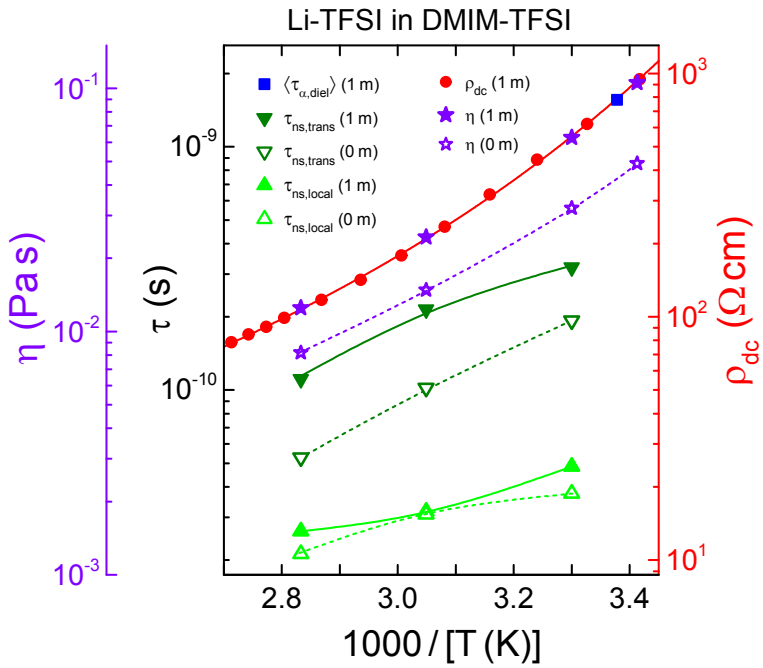

Fig. 10. Comparison of the temperature-dependent relaxation times of DMIM-TFSI without and with Li-TFSI (2nd left axis) with the dc resistivity (right axis) and viscosity (1st left axis), all shown in Arrhenius representation. Only the high-temperature range covered by the neutron-scattering experiments is shown (see Fig. 9 for ρ_{dc} and $\tau_{\alpha,diel}$ in an extended temperature range). All three axis ranges were adapted to cover the same number of decades. In addition, the start values of the τ and η ordinates were chosen to achieve an approximate match of $\tau_{\alpha,diel}(1/T)$ (cf. Fig. 9) and $\eta(1/T)$ with the $\rho_{dc}(1/T)$ curve for the 1 m sample. Circles: resistivity for the IL with 1 m Li-TFSI; square: average α-relaxation time of the 1 m sample determined by dielectric spectroscopy; open and closed upright triangles: local relaxation times measured by neutron scattering for 0 and 1 m IL, respectively; open and closed inverted triangles: translational relaxation times for 0 and 1 m IL, respectively; open and closed stars: viscosity for 0 m and 1 m Li-TFSI, respectively. The lines are guides to the eye, except the one through the ρ_{dc} data, representing a VFT fit.

Clearly, all three ion species can contribute to the resistivity of this IL, whatsoever most likely with different weight. However, based on dielectric spectroscopy alone, no statement on these contributions can be made. Interestingly, as discussed above, the neutron-scattering results

provide access to the translational motion of mainly a single ion species only, the $DMIM^+$ cations. The relaxation times of the translational process, $\tau_{ns,trans}$, were derived (via $\tau_{ns,trans} \sim \frac{1}{Dq^2}$ with q = 0.8 $Å^{-1}$) from the corresponding diffusion coefficients determined by QENS for the 1 m ILs (Fig. 8a). They are shown by the inverted closed triangles in Figs. 9 and 10, the latter providing an expanded view of the high-temperature region. When taking into account the relation $\eta \propto \rho_{dc} \propto \tau_{\alpha,diel}$ (see discussion above) and using the same relative axis scaling of ρ_{dc} and τ as in Fig. 9, the dc-resistivity and viscosity data shown in Fig. 10 can be regarded as a reasonable high-temperature extrapolation of the relaxation time $\tau_{\alpha,diel}$, which characterizes the coupled reorientational and translational ionic motion. A comparison with the inverted closed triangles in Fig. 10 reveals that the translational relaxation measured by QENS is significantly faster than the dynamics measured by the other methods. This decoupling implies that the mobility of the $DMIM^+$ ion, primarily detected by the QENS measurements, is faster than that of the other ions. This is well consistent with the finding of faster cation motion in various ILs, including DMIM-TFSI, based on NMR investigations.[35,96] Interestingly, such a decoupling seems to be also present for the sample without any Li (cf. open stars and open inverted triangles in Fig. 10). The overall size of $DMIM^+$ is smaller than that of the $TFSI^-$ ion which may explain its higher mobility, even in the pure IL. As pointed out in ref. [10a], the ionic shape also seems to play a role. Of course, the Li^+ ion is by far smaller than the two other ions and, naively, a very high mobility may be expected for this ion. However, it can be assumed that its much higher ionic potential increases its interactions with the other ions and therefore considerably reduces its mobility (and that of the other ions; cf. Fig. 5 and its discussion).

The local process detected by QENS (upright triangles in Figs. 9 and 10) is significantly faster and has a clearly weaker temperature dependence than the coupled resistivity, viscosity, and α relaxation. It thus seems completely unrelated to the ionic charge transport and may be ascribed to local motions within a transient cage formed by the nearest neighbors as discussed above (cf. Fig. 6 and its discussion). Such fast motions play a prominent role in the mode coupling theory (MCT) of the glass transition[40] and are a well-established experimental finding in spectra of glass forming liquids as measured, e.g., by neutron scattering.[45] Caged motion is also considered in other theoretical approaches, such as the coupling model.[46]

Finally, the diamonds in Fig. 9 indicate the Johari-Goldstein β relaxation times $\tau_{\beta,\mathrm{diel}} = 1/(2\pi\nu_p)$, determined by reading off the peak positions ν_p in the dielectric loss spectra shown in Fig. 3b and (in more detail) in Fig. 4a. Perfect Arrhenius behavior is found, which is typical for secondary relaxation processes. A linear fit (dash-dotted line) reveals an energy barrier $E_\beta \approx 0.44$ eV and a relatively small prefactor $\tau_0 \approx 10^{-16}$ s. In a related imidazolium-based IL with $TFSI^-$ anion, an activation energy of the JG relaxation of similar magnitude was found (0.38 eV).[21e] Interestingly, just as in this material, in our 1 m IL the relation $E_\beta = 24\ k_B T_g$ is well fulfilled when using $T_G \approx 208$ K determined from the DSC measurements (Fig. 1). This empirical relation was found to be valid in various molecular glass formers.[24a]

Conclusion

By performing neutron-scattering, dielectric, and viscosity measurements we have thoroughly characterizd the ionic dynamics in the liquid and supercooled state of a typical imidazolium-based IL with added Li^+ ions. By dielectric spectroscopy, two relaxational processes

have been detected, which resemble the typical α-β-relaxation scenario, well known from molecular glass formers. We ascribe them to the reorientational motions of the dipolar ions and the corresponding Johari-Goldstein β relaxation. We find a close coupling of the reorientational α relaxation to the viscosity and to the overall translational ionic motion associated with dc charge transport. Obviously, the temperature dependence of the ionic conductivity is dominated by a variation of ion dynamics exhibiting typical glasslike behavior and not by a temperature-dependent ionicity due to the formation of ion aggregates. Even at relatively high Li concentrations, the lithium-salt-doped ionic liquid investigated here still shows a high conductivity that is comparable to those of organic liquid electrolytes used in lithium-ion batteries and implies relatively fast ion diffusion.

By QENS, two distinct diffusion coefficients for the $DMIM^+$ ions were detected. The slower process is ascribed to translational diffusion of $DMIM^+$ and the faster process is identified as more local dynamic component, which is confirmed by the NSE data. A comparison with the dielectric, dc, and viscosity results indicates that the translational motion of the $DMIM^+$ ions is faster than the dynamics of the other ions and increasingly decouples from the general ionic dynamics at low temperatures. This finding is consistent with earlier NMR investigations[10a, 47] and nicely demonstrates that not only the size but also the shape and the ionic potential of an ion determine its mobility. Analysis of the NSE data further suggests that the Li^+ ions move over relatively long distances together with their first coordination shell and that the $DMIM^+$ cations may have a slightly higher net diffusion coefficient than the ion aggregates. The almost constant diffusion rate as a function of momentum transfer of the 1 m IL as measured by NSE suggests that ion aggregates (the vehicle diffusion mechanism) play an important role in the ion diffusion. The local

diffusion process detected by QENS exhibits a weaker dependence upon the salt concentration, temperature, and bulk viscosity, and clearly plays a minor role in the overall charge transport.

Acknowledgements:

This work was supported by the U.S. Department of Energy, Office of Science, Basic Energy Sciences, Materials Sciences and Engineering Division. The neutron scattering experiments at Oak Ridge National Laboratory's (ORNL) Spallation Neutron Source were supported by the Scientific User Facilities Division, Office of Basic Energy Sciences, U.S. Department of Energy (DOE). ORNL is managed by UTBattelle, LLC, for the U.S. DOE under Contract No. DE-AC05-00OR22725. The work in Augsburg was supported by the Deutsche Forschungsgemeinschaft (Grant No. LU 656/3-1) and by the BMBF via ENREKON.

References

[1] aM. Watanabe, M. L. Thomas, S. G. Zhang, K. Ueno, T. Yasuda, K. Dokko, *Chem. Rev.* **2017**, *117*, 7190-7239; bN. V. Plechkova, K. R. Seddon, *Chem. Soc. Rev.* **2008**, *37*, 123-150; cZ. Ma, J. H. Yu, S. Dai, *Adv. Mater.* **2010**, *22*, 261-285; dS. J. Zhang, J. Sun, X. C. Zhang, J. Y. Xin, Q. Q. Miao, J. J. Wang, *Chem. Soc. Rev.* **2014**, *43*, 7838-7869; eD. R. MacFarlane, N. Tachikawa, M. Forsyth, J. M. Pringle, P. C. Howlett, G. D. Elliott, J. H. Davis, M. Watanabe, P. Simon, C. A. Angell, *Energy Environ. Sci.* **2014**, *7*, 232-250; fM. Armand, F. Endres, D. R. MacFarlane, H. Ohno, B. Scrosati, *Nat. Mater.* **2009**, *8*, 621-629; gQ. W. Yang, Z. Q. Zhang, X. G. Sun, Y. S. Hu, H. B. Xing, S. Dai, *Chem. Soc. Rev.* **2018**, *47*, 2020-2064; hF. Lo Celso, Y. Yoshida, F. Castiglione, M. Ferro, A. Mele, C. J. Jafta, A. Triolo, O. Russina, *Phys. Chem. Chem. Phys.* **2017**, *19*, 13101-13110; iO. Russina, F. Lo Celso, N. Plechkova, C. J. Jafta, G. B. Appetecchi, A. Triolo, *Top. Curr. Chem.* **2017**, *375*.

[2] aA. Lewandowski, A. Swiderska-Mocek, *J. Power Sources* **2009**, *194*, 601-609; bG. A. Giffin, *J. Mater. Chem. A* **2016**, *4*, 13378-13389; cX. G. Sun, X. Q. Wang, R. T. Mayes, S. Dai, *Chemsuschem* **2012**, *5*, 2079-2085; dH. B. Xing, C. Liao, Q. W. Yang, G. M. Veith, B. K. Guo, X. G. Sun, Q. L. Ren, Y. S. Hu, S. Dai, *Angew. Chem. Int. Ed.* **2014**, *53*, 2099-2103; eM. Hog, B. Burgenmeister, K. Bromberger, M. Schuster, S. Riedel, I. Krossing, *Chemelectrochem* **2017**, *4*, 2934-2942; fX. G. Sun, C. Liao, N. Shao, J. R. Bell, B. K. Guo, H. M. Luo, D. E. Jiang, S. Dai, *J. Power Sources* **2013**, *237*, 5-12; gD. J. Yoo, J. S. Kim, J. Shin, K. J. Kim, J. W. Choi, *Chemelectrochem* **2017**, *4*, 2345-2351; hX. G. Sun, Z. Z. Zhang, H. Y. Guan, C. A. Bridges, Y. X. Fang, Y. S. Hu, G. M. Veith, S. Dai, *J. Mater. Chem. A* **2017**, *5*, 6589-6596; iX. G. Sun, Z. H. Bi, H. S. Liu, Y. X. Fang, C. A. Bridges, M. P. Paranthaman, S. Dai, G. M. Brown, *Chem. Commun.* **2016**, *52*, 1713-1716; jC. A. Bridges, X. G.

Sun, B. K. Guo, W. T. Heller, L. L. He, M. P. Paranthaman, S. Dai, *Acs Energy Letters* **2017**, *2*, 1698-1704.

[3] aC. Liao, N. Shao, K. S. Han, X. G. Sun, D. E. Jiang, E. W. Hagaman, S. Dai, *Phys. Chem. Chem. Phys.* **2011**, *13*, 21503-21510; bK. Hayamizu, Y. Aihara, H. Nakagawa, T. Nukuda, W. S. Price, *J. Phys. Chem. B* **2004**, *108*, 19527-19532.

[4] aT. Fromling, M. Kunze, M. Schonhoff, J. Sundermeyer, B. Roling, *J. Phys. Chem. B* **2008**, *112*, 12985-12990; bF. F. Chen, M. Forsyth, *Phys. Chem. Chem. Phys.* **2016**, *18*, 19336-19344; cM. Forsyth, G. M. A. Girard, A. Basile, M. Hilder, D. R. MacFarlane, F. Chen, P. C. Howlett, *Electrochim. Acta* **2016**, *220*, 609-617.

[5] aZ. Li, G. D. Smith, D. Bedrov, *J. Phys. Chem. B* **2012**, *116*, 12801-12809; bO. Borodin, G. D. Smith, W. Henderson, *J. Phys. Chem. B* **2006**, *110*, 16879-16886; cJ. B. Haskins, C. W. Bauschlicher, J. W. Lawson, *J. Phys. Chem. B* **2015**, *119*, 14705-14719.

[6] aJ. Pitawala, A. Martinelli, P. Johansson, P. Jacobsson, A. Matic, *J. Non-Crystalline Solids* **2015**, *407*, 318-323; bL. J. Hardwick, M. Holzapfel, A. Wokaun, P. Novak, *J. Raman Spectrosc.* **2007**, *38*, 110-112; cJ. C. Lassegues, J. Grondin, C. Aupetit, P. Johansson, *J. Phys. Chem. A* **2009**, *113*, 305-314.

[7] aF. Castiglione, E. Ragg, A. Mele, G. B. Appetecchi, M. Montanino, S. Passerini, *J. Phys. Chem. Lett.* **2011**, *2*, 153-157; bK. Hayamizu, S. Tsuzuki, S. Seki, *J. Chem. Eng. Data* **2014**, *59*, 1944-1954.

[8] M. Gouverneur, J. Kopp, L. van Wullen, M. Schonhoff, *Phys. Chem. Chem. Phys.* **2015**, *17*, 30680-30686.

[9] M. L. P. Le, F. Alloin, P. Strobel, J. C. Lepretre, C. P. del Valle, P. Judeinstein, *J. Phys. Chem. B* **2010**, *114*, 894-903.

[10] aH. Tokuda, K. Hayamizu, K. Ishii, M. Susan, M. Watanabe, *J. Phys. Chem. B* **2005**, *109*, 6103-6110; bC. W. Do, X. G. Sun, C. J. Jafta, S. Dai, M. Ohl, E. Mamontov, *Sci. Rep.* **2018**, *8*, 10354.

[11] P. Sippel, V. Dietrich, D. Reuter, M. Aumüller, P. Lunkenheimer, A. Loidl, S. Krohns, *J. Mol. Liq.* **2016**, *223*, 635.

[12] aR. Böhmer, M. Maglione, P. Lunkenheimer, A. Loidl, *J. Appl. Phys.* **1989**, *65*, 901-904; bP. Lunkenheimer, U. Schneider, R. Brand, A. Loid, *Contemp. Phys.* **2000**, *41*, 15-36.

[13] M. Ohl, M. Monkenbusch, N. Arend, T. Kozielewski, G. Vehres, C. Tiemann, M. Butzek, H. Soltner, U. Giesen, R. Achten, H. Stelzer, B. Lindenau, A. Budwig, H. Kleines, M. Drochner, P. Kaemmerling, M. Wagener, R. Möller, E. B. Iverson, M. Sharp, D. Richter, *Nuclear Instruments and Methods in Physics Research Section A: Accelerators, Spectrometers, Detectors and Associated Equipment* **2012**, *696*, 85-99.

[14] E. Mamontov, K. W. Herwig, *Rev Sci Instrum* **2011**, *82*, 085109.

[15] aW. Xu, L. M. Wang, R. A. Nieman, C. A. Angell, *J. Phys. Chem. B* **2003**, *107*, 11749-11756; bC. A. Angell, Y. Ansari, Z. F. Zhao, *Faraday Discuss.* **2012**, *154*, 9-27.

[16] H. Matsumoto, H. Sakaebe, K. Tatsumi, M. Kikuta, E. Ishiko, M. Kono, *J. Power Sources* **2006**, *160*, 1308-1313.

[17] aH. Vogel, *Phys. Z.* **1921**, *22*, 645; bG. S. Fulcher, *J. Am. Ceram. Soc.* **1923**, *8*, 339-355; cG. Tammann, W. Hesse, *Z Anorg Allg Chem* **1926**, *156*, 245-257; dC. A. Angell, in *National Technical Information Service*, Springfield, **1985**, p. 3; eM. D. Ediger, C. A. Angell, S. R. Nagel, *J. Phys. Chem.* **1996**, *100*, 13200-13212.

[18] aG. Adam, J. H. Gibbs, *The Journal of Chemical Physics* **1965**, *43*, 139-146; bM. Galinski, A. Lewandowski, I. Stepniak, *Electrochimica Acta* **2006**, *51*, 5567-5580.

[19] S. Emmert, M. Wolf, R. Gulich, S. Krohns, S. Kastner, P. Lunkenheimer, A. Loidl, *Eur. Phys. J. B* **2011**, *83*, 157.

[20] aP. Lunkenheimer, A. Loidl, *Chem. Phys.* **2002**, *284*, 205-219; bA. Schönhals, F. Kremer, in *Broadband Dielectric Spectroscopy* (Eds.: F. Kremer, A. Schönhals), Springer Berlin Heidelberg, Berlin, Heidelberg, **2003**, pp. 35-57.
[21] aP. Sippel, P. Lunkenheimer, S. Krohns, E. Thoms, A. Loidl, *Sci Rep* **2015**, *5*, 13922; bE. Thoms, P. Sippel, D. Reuter, M. Weiß, A. Loidl, S. Krohns, **2017**, https://arxiv.org/ftp/arxiv/papers/1703/1703.05625.pdf ; cC. Krause, J. Sangoro, C. Iacob, F. Kremer, *J. Phys. Chem. B* **2009**, *114*, 382-386; dA. Rivera, A. Brodin, A. Pugachev, E. Rössler, *J. Chem. Phys.* **2007**, *126*, 114503; eA. Rivera, E. A. Rössler, *Phys. Rev. B* **2006**, *73*, 212201; fJ. Hunger, A. Stoppa, S. Schrödle, G. Hefter, R. Buchner, *ChemPhysChem* **2009**, *10*, 723-733; gC. Gainaru, E. W. Stacy, V. Bocharova, M. Gobet, A. P. Holt, T. Saito, S. Greenbaum, A. P. Sokolov, *J. Phys. Chem. B* **2016**, *120*, 11074-11083.
[22] P. Sippel, P. Lunkenheimer, S. Krohns, E. Thoms, A. Loidl, *Sci. Rep.* **2015**, *5*.
[23] P. J. Griffin, A. L. Agapov, A. P. Sokolov, *Phys. Rev. E* **2012**, *86*, 021508.
[24] aA. Kudlik, S. Benkhof, T. Blochowicz, C. Tschirwitz, E. Rössler, *J. Mol. Struct.* **1999**, *479*, 201-218; bS. Kastner, M. Köhler, Y. Goncharov, P. Lunkenheimer, A. Loidl, *J. Non-Crystal. Solids* **2011**, *357*, 510-514.
[25] G. P. Johari, M. Goldstein, *J. Chem. Phys.* **1970**, *53*, 2372-2388.
[26] aF. H. Stillinger, *Science* **1995**, *267*, 1935-1939; bJ. S. Harmon, M. D. Demetriou, W. L. Johnson, K. Samwer, *Phys. Rev.lett.* **2007**, *99*, 135502.
[27] D. W. Davidson, R. H. Cole, *J. Chem. Phys.* **1951**, *19*, 1484-1490.
[28] P. Macedo, *Phys. Chem. Glasses* **1972**, *13*, 171-179.
[29] aN. Ito, W. Huang, R. Richert, *J. Phys. Chem. B* **2006**, *110*, 4371-4377; bG. Jarosz, M. Mierzwa, J. Zioło, M. Paluch, H. Shirota, K. Ngai, *J. Phys. Chem. B* **2011**, *115*, 12709-12716.
[30] aS. Elliott, *J. non-crystal. solids* **1994**, *170*, 97-100; bB. Roling, *J. non-crystal. solids* **1999**, *244*, 34-43; cI. Hodge, K. Ngai, C. Moynihan, *J. non-crystal. solids* **2005**, *351*, 104-115.
[31] S. Seki, Y. Ohno, Y. Kobayashi, H. Miyashiro, A. Usami, Y. Mita, H. Tokuda, M. Watanabe, K. Hayamizu, S. Tsuzuki, M. Hattori, N. Terada, *J. Electrochem. Soc.* **2007**, *154*, A173-A177.
[32] C. A. Angell, *Electrochimica Acta* **2017**, *250*, 368-375.
[33] Z. Wojnarowska, Y. Wang, K. J. Paluch, A. P. Sokolov, M. Paluch, *Phys. Chem. Chem. Phys.* **2014**, *16*, 9123-9127.
[34] X. G. Sun, S. Wan, H. Y. Guang, Y. X. Fang, K. S. Reeves, M. F. Chi, S. Dai, *J. Mater. Chem. A* **2017**, *5*, 1233-1241.
[35] L. Liang, R. Rinaldi, H. Schober, *Neutron Applications in Earth, Energy and Environmental Sciences*, Springer US, Boston, MA, **2009.**
[36] E. Mamontov, H. Luo, S. Dai, *J Phys Chem B* **2009**, *113*, 159-169.
[37] M. C. Bellissent-Funel, S. H. Chen, J. M. Zanotti, *Physical Review E* **1995**, *51*, 4558-4569.
[38] E. Mamontov, G. A. Baker, H. Luo, S. Dai, *Chemphyschem* **2011**, *12*, 944-950.
[39] A. Triolo, O. Russina, V. Arrighi, F. Juranyi, S. Janssen, C. M. Gordon, *J. Chem. Phys.* **2003**, *119*, 8549-8557.
[40] W. Gotze, L. Sjogren, *Reports on progress in Physics* **1992**, *55*, 241.
[41] aP. G. Debenedetti, F. H. Stillinger, *Nature* **2001**, *410*, 259; bT. Kirkpatrick, P. Wolynes, *Phys. Rev. B* **1987**, *36*, 8552; cT. Bauer, P. Lunkenheimer, A. Loidl, *Phys. Rev. lett.* **2013**, *111*, 225702.
[42] M. Köhler, P. Lunkenheimer, A. Loidl, *Eur. Phys. J. E* **2008**, *27*, 115.
[43] aK. Geirhos, P. Lunkenheimer, M. Michl, D. Reuter, A. Loidl, *J Chem Phys* **2015**, *143*, 081101; bD. Reuter, C. Geiß, P. Lunkenheimer, A. Loidl, *J. Chem. Phys.* **2017**, *147*, 104502.
[44] D. R. MacFarlane, M. Forsyth, E. I. Izgorodina, A. P. Abbott, G. Annat, K. Fraser, *Phys. Chem. Chem. Phys.* **2009**, *11*, 4962-4967.

[45] aW. Knaak, F. Mezei, B. Farago, *EPL (Europhysics Letters)* **1988**, *7*, 529; bJ. Wuttke, J. Hernandez, G. Li, G. Coddens, H. Cummins, F. Fujara, W. Petry, H. Sillescu, *Phys. Rev. Lett.* **1994**, *72*, 3052.
[46] K. Ngai, *J. Phys.: Condens. Matt.* **2003**, *15*, S1107.
[47] H. Every, A. Bishop, M. Forsyth, D. MacFarlane, *Electrochimica Acta* **2000**, *45*, 1279-1284.